J Clust Sci (2016) 27:227–239
DOI 10.1007/s10876-015-0924-4

ORIGINAL PAPER

Facile Synthesis of Fe_xO_y/Ag Nanocomposites for Multifunctional and Efficient Catalytic Applications

Li Zhang[1] · Jing Li[1] · Xikun Chu[1] · Guang-chao Zhao[1]

Received: 14 March 2015 / Published online: 16 September 2015

Abstract In this study, the iron oxide/silver (Fe_xO_y/Ag) nanocomposite has been successfully prepared by a facile one-step method using goethite (α-FeOOH) rods as support. The diameter of the as-synthesized goethite rods was between 250 and 500 nm and the silver nanoparticles sizes were about 10–50 nm. By varying the concentrations, the Fe_xO_y/Ag nanocomposite with different Ag contents are successfully obtained. The Fe_xO_y/Ag nanocomposite was characterized by scanning electron microscopy, transmission electron microscopy, X-ray diffraction, and energy dispersive spectroscopy, respectively. Due to the unique nanostructure, these nanocomposites can catalyze degradation of both aromatic nitro compounds and organic dyes only within a few minutes, which show high catalytic performance.

Keywords Goethite rods · Ag nanoparticles · Nanocomposites · Aromatic nitro compounds · Organic dyes

Introduction

As one of the members of the noble metallic nanomaterials family, silver nanoparticles have sparked intense excitement in nanotechnology due to their high catalytic activity. For instance, they can be used as catalysts for the reduction of organics [1, 2], for fuel cells [3], in surface-enhanced Raman scattering [4, 5], in antibacterial material [6], and in electrode [7]. However, their high surface energy

Electronic supplementary material The online version of this article (doi:10.1007/s10876-015-0924-4) contains supplementary material, which is available to authorized users.

✉ Guang-chao Zhao
gczhao@mail.ahnu.edu.cn

[1] College of Chemistry and Materials Science, Anhui Key Laboratory of Functional Molecular Solids, Anhui Normal University, Wuhu 241000, People's Republic of China

resulting from the high surface-to-volume ratio undesirably causes serious stability problem. They tend to easily change shape, aggregate and damage the surface states during catalytic reactions, and lose their inherent catalytic activity [8–12]. In order to disperse silver nanoparticles and to improve their catalytic efficiency, carbon [13–15], metal oxides [16, 17] or silica [18] are usually used as supports.

Goethite is one of coarse polymorphs of iron oxyhydroxide and widespread in the natural environment. The structure is composed of double chains of iron in octahedral oxygen co-ordination, which are further linked by sharing vertices in a three-dimensional framework structure [19]. Goethite (α-FeOOH) can be used as a pigment and is the most important precursor in the synthesis of iron oxides such as hematite (α-Fe_2O_3) and maghemite (γ-Fe_2O_3) [20–22]. In addition, goethite particles have high specific surface areas and strong affinities for heavy metals like Tin [23] and oxyanions, such as oleic acid [24], humic acid [25], pyromellitic acid [26], trimethyl phosphate [27], and sulfate [28]. Citrate ions are ligands for chelate or complex formation with metal ions and are used as a masking agent in analytical chemistry. According to the literature, we can know that citrate ions can inhibit the formation and crystallization of ferric oxide hydroxide particles, and their particle sizes decreased with increase in the concentration of these ions [29]. Moreover, in presence of citrate, metal (like nickel [30]) can be adsorbed to goethite. Despite those, very few studies have been reported on synthesize the FeOOH/noble metal nanoparticle composites. Calvar and co-workers [31] report a procedure for growing Au shells on goethite rods by SiO_2-mediated assembly of Au nanoparticles.

In very recent years, the use of synthesized nanocomposite materials in catalytic applications has made great progress. In literature, to examine the catalytic performance of Ag nanocomposites, the reduction of aromatic nitro compounds and organic dyes with an excess amount of sodium borohydride has often been used as a model reaction [14, 32, 33]. The product of aromatic nitro compounds, 4-aminophenol and 4-phenylenediamine, are attractive industrial intermediate for preparation of polymers, drugs, anticorrosion lubricants, hair dyes, and rubber products [11, 34]. It is therefore highly desirable to develop more efficient, durable and eco-friendly catalytic systems to produce them. Currently, most organic dyes are synthetic compounds, which have become one of the main sources of environment pollution due to their toxicity and resistant to the aerobic degradation [14, 33]. Therefore, it is also important to investigate the catalytic degradation for organic dyes. In the study, p-nitroaniline, p-nitrophenol, Rhodamine B and Rhodamine 6G were chosen as model nitro compounds and dyes to evaluate the catalytic activity of the as fabricated Fe_xO_y–Ag nanocomposite.

In this study, we report a new and simple procedure for growing Ag nanoparticles on goethite rods. Firstly, FeOOH was modified by sodium citrate. Then, citrate ions were used to attach Ag ions onto the surface of FeOOH through electrostatic interaction. Subsequently, the Ag ions were reduced by $NaBH_4$. Without a repeated coating process, Ag nanoparticle can be formed on the goethite rods surface by only one step. Further, the multifunctional and efficient catalytic activity of the Fe_xO_y/Ag nanocomposite was explored using the reduction system of aromatic nitro compounds and organic dyes as model reactions.

Experimental

Materials

Sodium borohydride ($NaBH_4$) (Sigma Aldrich), NaOH, $FeCl_3{\cdot}6H_2O$, silver nitrate ($AgNO_3$), trisodium citrate dehydrate, p-nitroaniline, p-nitrophenol, Rhodamine B, and Rhodamine 6G were obtained from Shanghai Chemical Reagent Company. All reagents were used as received without further purification. All the chemicals were analytical grade.

Synthesis of Goethite Nanorods

Goethite nanorods were prepared according to the previous method [35]. 0.5 g $FeCl_3{\cdot}6H_2O$ and 0.5 g NaOH were separately put into 15 mL of water with vigorous stirring and then mixed. After stirring for 10 min, the solution was transferred to a Teflon-lined stainless-steel autoclave (40 mL) and heated at 180°C for 4 h.

Preparation of the Fe_xO_y/Ag Nanocomposite

Sodium citrate solution (0.3 mL, 0.5 mM) and 5 mg FeOOH was mixed with stirring about 5 min, then silver nitrate (7.5 mM) was added with vigorous stirring about 5 min at room temperature. After freshly prepared sodium borohydride (0.3 mL, 10 mM) was mixed with above aqueous solution with ultrasonication for 30 min, the solution was remained stirring for 24 h. Finally, the solution was centrifuged and washed with ethanol and water 3 times, respectively.

Characterization of the Fe_xO_y/Ag Nanocomposite

The X-ray powder diffraction pattern of the samples was characterized on a Shimadzu XRD-6000 X-ray diffractometer with Cu Kα radiation ($\lambda = 1.54060$ Å) at a scanning rate of 0.05 deg s^{-1} and 2θ ranges from 10° to 80°. The Transmission electron microscopy (TEM) images were obtained on a JEOL JEM-200CX high resolution transmission electron microscope, employing an accelerating voltage of 200 kV. The scanning electron microscope (SEM) and energy dispersive X-ray (EDS) images were obtained on Hitachi S-4800 field emission scanning electron microscope with an accelerating voltage of 5 and 15 kV, respectively. The Fourier transform infrared spectrophotometer (FT-IR) spectra were collected in the transmission mode (4000–450 cm^{-1}) using a FT-IR instrument (IRPrestige-21, SHIMADZU, Japan). The samples were prepared in a pellet form with spectroscopic-grade KBr. UV–Vis absorption spectra were recorded at room temperature on a Metash UV-6100s spectrophotometer.

Catalytic Reduction Measurement

The catalytic reduction experiments was conducted with Fe_xO_y/Ag as the catalyst in freshly prepared aqueous solution of $NaBH_4$ (2.0 mL, 0.068 M) mixed with

p-nitrophenol (0.4 mL, 1.0 mM) or p-nitroaniline (0.4 mL, 1.0 mM) or rhodamine B (0.4 mL, 1.0×10^{-2} mM) or Rhodamine 6G (0.4 mL, 1.2×10^{-2} mM) in the quartz cell (1.0 cm path length and 4 mL volume). For comparison, the same experiment with Ag nanoparticles or pure FeOOH (100 μL, 0.2 g/L) was also carried out. The variation of concentration was measured with a Metash UV-6100s spectrophotometer.

Results and Discussion

Structure and Morphology Characterization

Scheme 1 shows the schematic illustration for the synthesis of the uniform Fe_xO_y/Ag nanocomposites. A great deal of hydroxyl groups can be found from the structural of FeOOH [36]. At the beginning, the sodium citrate was added to the

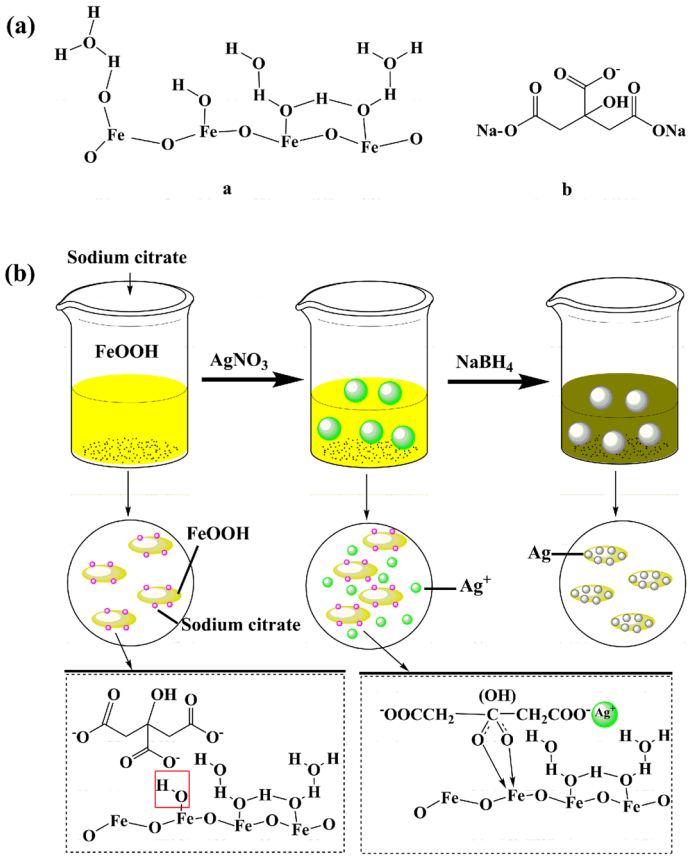

Scheme 1 **a** Structural of *a* FeOOH and *b* sodium citrate. **b** Schematic of the fabrication process of the Fe_xO_y/Ag nanocomposite

aqueous solution of FeOOH nanorods. Part of the carboxy groups of sodium citrate can replace the hydroxyl groups of FeOOH [24]. By means of single-sorbate sorption, the citrate with negative charges was linked to the surface of FeOOH, which is profitable for anchoring Ag^+ onto the surface of the FeOOH through electrostatic interaction. Subsequently, the Ag^+ were reduced by $NaBH_4$ solution in one step. In this way, the Fe_xO_y/Ag nanocomposite was obtained. The occurrence of interaction between citrate and Ag^+ is profitable for immobilization of Ag nanoparticles and thereby prevents the newly agglomeration of Ag nanoparticles.

The typical X-ray diffraction (XRD) patterns of Fe_xO_y/Ag and FeOOH are illustrated in Fig. 1a. All peaks of the as-synthesized FeOOH nanorods are in good agreement with the standard profiles of orthorhombic α-FeOOH (goethite, JCPDS No. 29-0713, space group Pnma, a = 9.95 Å, b= 3.01 Å, c = 4.62 Å) [21]. After deposited with Ag, new peaks located at 2θ = 37.7°, 43.9°, 64.2° and 77.1° corresponding to the reflections of (111), (200), (220), and (311) crystalline planes of the fcc structure of Ag (JCPDS No.04-0783) appeared respectively. While the peaks at 21.22°, 55.31°, and 57.32° were attributed to as-synthesized FeOOH. The remaining peaks were attributed to the $Fe_{23.333}O_{32}$ (Iron Oxide, JCPDS No. 76-1470). As a comparison, the XRD of FeOOH with $NaBH_4$ was also provided, which is shown in Fig. S1. It indicated that the transformation form FeOOH into $Fe_{23.333}O_{32}$ did not attributed to $NaBH_4$. Energy dispersive analysis of X-rays of selected areas (EDS; Fig. 1b) of the Fe_xO_y/Ag nanocomposite further reveals their elemental composition. Fe, Ag, O, and C can be easily found in the EDS graph. Among those elements, the peaks of C and O confirm the presence of the sodium citrate. Fe and Ag signals result from FeOOH and Ag.

In addition, the FT-IR spectra of the samples were obtained in Fig. 2, with curves corresponding to FeOOH, sodium citrate, FeOOH/sodium citrate and the Fe_xO_y/Ag nanocomposites, respectively. As for FeOOH, before adding sodium citrate, the characteristic stretching vibration was the board peak at 3200 cm^{-1}, which was ascribed to O–H groups. The deformational modes of hydroxyls (out-of-plane around 780–800 cm^{-1} and in-plane around 880–900 cm^{-1}) [37] typical for goethite are well-defined in the syntheses of FeOOH nanorods. Conversely, when sodium

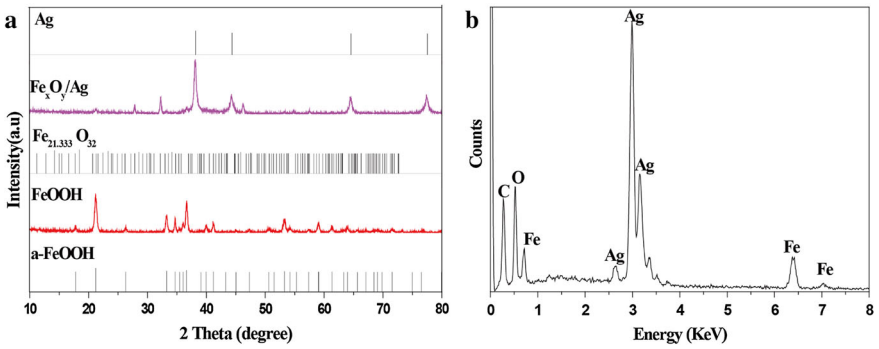

Fig. 1 XRD image (**a**) and EDS pattern (**b**) of the Fe_xO_y/Ag nanocomposite

citrate was added, these deformational modes of hydroxyls were weak. Compared with the FeOOH nanorods, it is observed that the typical C=O asymmetric stretching vibration at 1636 and 1579 cm^{-1}, and the fingerprint area (1250–800 cm^{-1}) are well in agreement to citrate reference spectra [38]. These results indicated that the surface of FeOOH was functionalized with citrate. After the Ag^{+} was reduced, the characteristic absorption of the O–H stretching peak disappeared, observations suggest that most of the hydroxyls had been removed.

The morphology of the product was characterized by scanning electron microscopy (SEM) and transition electron microscopy (TEM). From the images shown in Fig. 3a and b, we can see that the Ag nanoparticles with size of 10–50 nm were well coated on the surface of the FeOOH nanorod and no isolated nanoparticles were observed, which indicates that the high-quality Fe_xO_y/Ag nanocomposite was formed. The selected-area electron diffraction (SAED) pattern shows the presence of spots due to Ag, $Fe_{21.333}O_{32}$ and FeOOH (the inset in Fig. 3c). The high-resolution TEM (HRTEM) image (Fig. 3d) shows the existence of the FeOOH layers, $Fe_{21.333}O_{32}$ layers and the crystalline lattices could be attributed to (111) phases (d = 0.235 nm) of Ag. In contrast, the exact same synthesis strategy produced aggregated Ag nanoparticles with a diameter of 20–100 nm in the absence of FeOOH as the supports (Fig. S2). These particles aggregated with each other. Such morphological difference highlights the important role of FeOOH as a useful support for mediating the uniform growth of other functional nanomaterials.

To gain further insight into the factors that can influence the coverage of silver nanoparticles on the FeOOH nanorods, a control experiment was performed. Figures 4a–d show the SEM images of the uniform Fe_xO_y/Ag nanocomposites with different Ag contents, which are 0, 40, 70, and 80 wt%, respectively. As shown in Fig. 4a, the FeOOH rods exhibit homogeneously-distributed diameters in the range of 250–500 nm. In addition, it can be seen that with the increase of the mass ratio of $AgNO_3$ and FeOOH, Ag nanoparticles are clearly seen on the surface Fe_xO_y rods, and the density gradually increases. Moreover, the diameter of the Ag nanoparticles also increases. Ag nanoparticles were all uniformly distributed on the nanorods and did not aggregate with each other to form large clusters (Fig. 4c). When the Ag

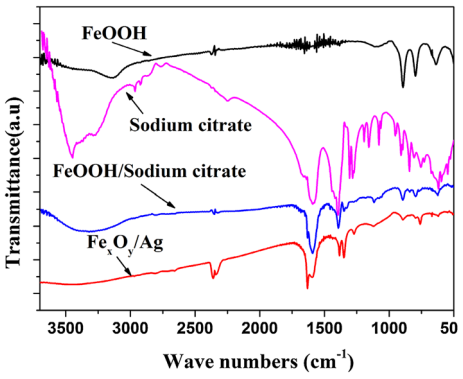

Fig. 2 FT-IR spectra of FeOOH nanorods, sodium citrate, FeOOH/sodium citrate and Fe_xO_y/Ag nanocomposites

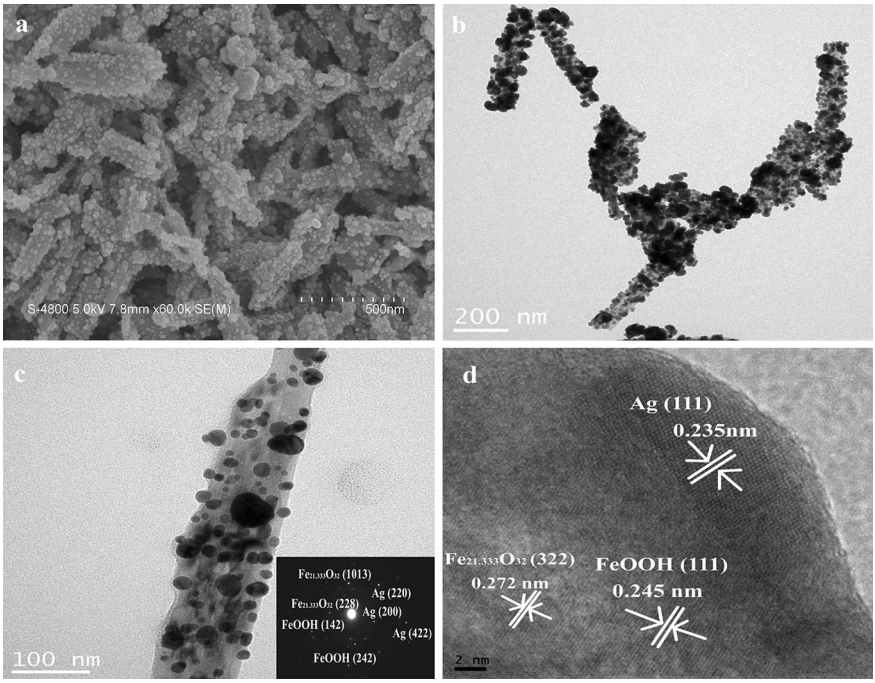

Fig. 3 Morphological and structural characterizations of uniform Fe_xO_y/Ag nanocomposites: **a** SEM image, **b**, **c** TEM images (*inset*: the selected area electron diffraction image), **d** HRTEM image

content increases to 80 wt%, all of the Fe_xO_y were completely coated by the Ag nanoparticles (Fig. 4d), and the isolated Ag nanoparticles were also observed. In addition, we found that sodium citrate plays an important role in the synthesis of the uniform Fe_xO_y/Ag nanocomposite. Figure 4e shows the SEM image of the Fe_xO_y/Ag nanocomposites without sodium citrate. It is clearly seen that the silver nanoparticles were not successfully decorated on the surface of FeOOH. As a comparison, the SEM image of Fe_xO_y/Ag nanocomposite without $NaBH_4$ shows that no silver nanoparticles were found, indicating silver ions would not be reduced without $NaBH_4$.

Multifunctional and Efficient Catalytic Applications for Aromatic Nitro Compounds and Organic Dyes

The catalytic activity of these nanocomposites was investigated for the reduction of aromatic nitro compounds and organic dyes by using $NaBH_4$ as the reducing agent. This reduction procedure can be feasibly monitored by time-dependent UV–Vis absorption spectra.

Figures 5 and 6 show the results of the two aromatic nitro compounds, p-nitroaniline and p-nitrophenol, catalyzed by the synthesized nanocomposites. For the reduction of p-nitroaniline to p-phenylenediamine, the absorption intensity was

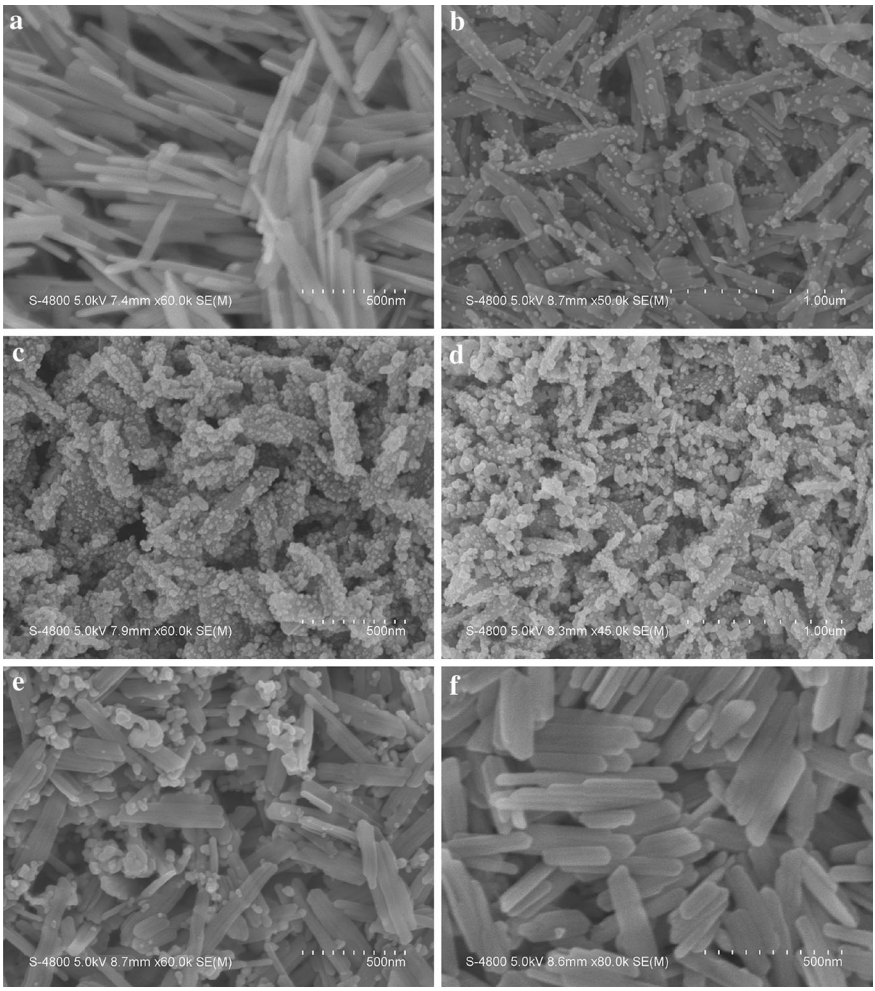

Fig. 4 SEM images of Fe_xO_y/Ag nanocomposites with different Ag content: **a** 0 wt%, **b** 40 wt%, **c** 70 wt%, and **d** 80 wt%. SEM images of Fe_xO_y/Ag nanocomposites without sodium citrate (**e**), and $NaBH_4$ (**f**)

almost unchanged after 4 h in the absence of the catalyst. Moreover, with only FeOOH or Ag nanoparticles as the catalyst, the reduction also did not proceed very quickly, even with excess of $NaBH_4$ (Fig. S4). In contrast, after addition of the Fe_xO_y/Ag catalyst into the system, the absorption intensity of p-nitroaniline at 378 nm decreased rapidly with time, which was accompanied by the appearance of the peak of p-phenylenediamine at 223 nm (Fig. 5b), indicating the successful transformation of p-nitroaniline to p-phenylenediamine. This reduction reaction could be completed within 4 min, evidently displayed by a rapid decolorization of the yellow-green solution (Fig. 5a).

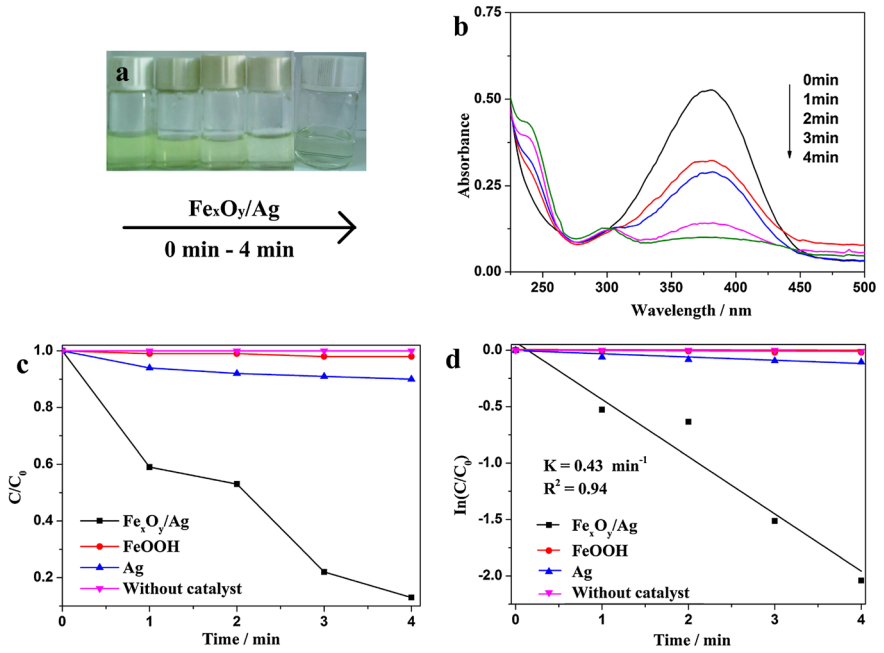

Fig. 5 **a** The photos of the corresponding solutions at various times. **b** UV–visible spectra for the chemical reduction of p-nitroaniline using Fe_xO_y/Ag nanocomposites as catalyst. **c** Plot of C/C_0 versus reaction time for the reduction of p-nitroaniline. **d** Relationship between $\ln(C/C_0)$ and reaction time t for the reduction using different catalysts

On the basis of the pseudo-first-order kinetics, $\ln(C/C_0) = -kt$, where C is the concentration of the p-nitroaniline at time t, C_0 is the initial concentration of the p-nitroaniline solution; and the slope k is the apparent reaction rate. The calculated rate constant for p-nitroaniline reduction with the Fe_xO_y/Ag nanocomposite in the presence of $NaBH_4$ is 0.42 min^{-1} (Fig. 5d). Similarly, the Fe_xO_y/Ag nanocomposite exhibited the good catalytic ability for reduction of p-nitrophenol, which has a different structure from p-nitroaniline (Fig. 6 and Fig. S3). Discarding the delay time, the plot very well follows the first-order reaction kinetics, with a correlation coefficient of 0.96. The rate constant k obtained directly from the slope of the straight line was 0.53 min^{-1} for Fe_xO_y/Ag. This value is higher than those of Ag@AMH (0.27 min^{-1}) [11], PS/Ag composite particle (0.21 min^{-1}) [32], and CNFs/AgNPs composite nanofibers (0.37 min^{-1}) [39], but lower than those of Fe_3O_4@SiO_2–Ag (0.83 min^{-1}) [40] and polyaniline nanofiber-supported Ag nanoparticles (1.28 min^{-1}) [41]. The difference of the catalytic activity between the currently developed Fe_xO_y/Ag nanocomposite and other Ag-based nanocomposites can be explained as follows: The good catalytic activities of the Fe_xO_y/Ag nanocomposite may be ascribed to the incorporated Fe_xO_y components. On one hand, the precursor of Fe_xO_y (FeOOH) with abundant –OH acts as a good platform to link the citrate with negative charges, which is profitable for anchoring Ag^+ onto

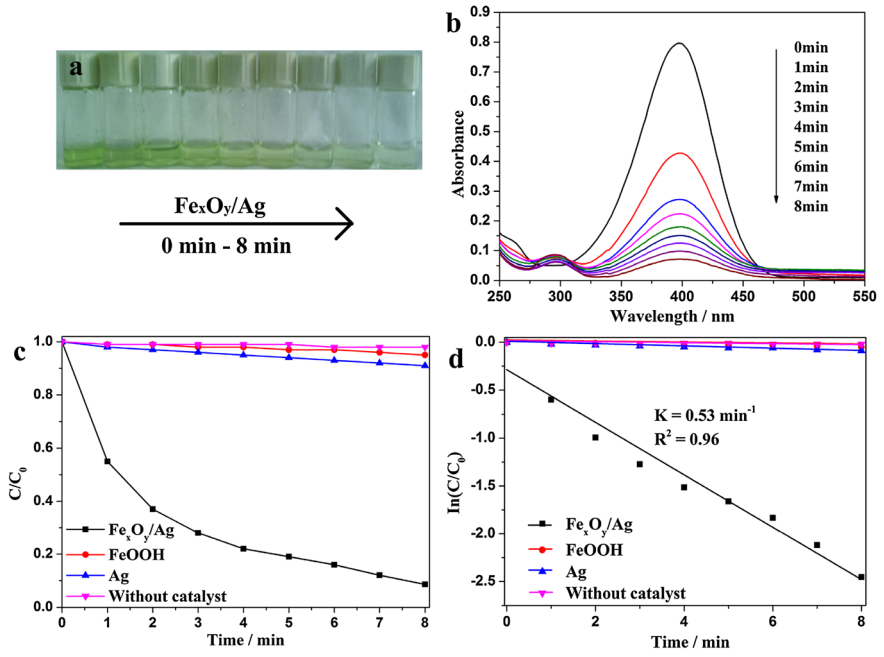

Fig. 6 **a** The photos of the corresponding solutions at various times. **b** UV–visible spectra for the chemical reduction of p-nitrophenol using Fe_xO_y/Ag nanocomposites as catalyst. **c** Plot of C/C_0 versus reaction time for the reduction of p-nitrophenol. **d** Relationship between $\ln(C/C_0)$ and reaction time t for the reduction using different catalysts

the surface of the FeOOH through electrostatic interactions. Herein, the aggregation of the Ag Nanoparticles (Ag NPs) is avoided by being densely coated onto the surface of Fe_xO_y. On the other hand, as reported in the previous literature, the region of electron transfer through the Ag NPs, is expanded with the aid of strong interactions between the substrate and Ag NPs. Therefore, the electron transfer between BH_4^- ions and p-nitrophenol molecule can occur quickly not only on the surface of Ag NPs but also on the interface of the Ag NPs and Fe_xO_y. Obviously, both situations can accelerate the reduction reaction of p-nitrophenol. Therefore, Fe_xO_y may play an active part in the catalysis and yield a synergistic effect, which leads to their better catalytic performance. As for their worse catalytic performance than Fe_3O_4@SiO_2–Ag and polyaniline nanofiber-supported Ag nanoparticles, it may be due to that (1) the silica coat on the surface of Fe_3O_4 not only is an effective substrate for immobilizing Ag NPs, but also improves the stability of Fe_3O_4 core [40]; (2) 4-NP can be adsorbed onto polyaniline nanofiber via π–π stacking interactions as it is π-rich in nature [41].

Generally, most of the organic dyes are synthetic compounds, which present a potential danger to the environment due to their toxicity and resistant to the aerobic degradation [42]. Therefore, degradation of the organic dyes is of special importance to the environmental protection. In this study, to evaluate the catalytic

ability of the Fe_xO_y/Ag nanocomposite in the degradation of organic dyes, Rhodamine B and Rhodamine 6G were chosen as the model dyes. Firstly, the progression of the catalytic reduction of RhB can be easily followed by the change in optical density at the wavelength of the absorption maximum ($\lambda = 553$ nm) of Rhodamine B. When the reaction system was added with the Fe_xO_y/Ag nanocomposite, the absorption peak of Rhodamine B quickly decreased and the reduction reaction was completed within 5 min (see Fig. 7b). This can be directly reflected from the optical photos, in which the fading and ultimate bleaching of Rhodamine B solutions in color appeared (Fig. 7a). For the sake of comparison, the catalytic activity of Ag or FeOOH was also examined at the same conditions and shown in Fig. S5. Very obviously, the reduction of Rhodamine B by only $NaBH_4$ hardly occurred in the absence of the catalysts. The similar phenomena occurred for the reduction of Rhodamine 6G (Fig. 8 and Fig. S6). These results strongly indicate that the Fe_xO_y/Ag nanocomposite has the good catalytic performance for the reduction of these organic dyes.

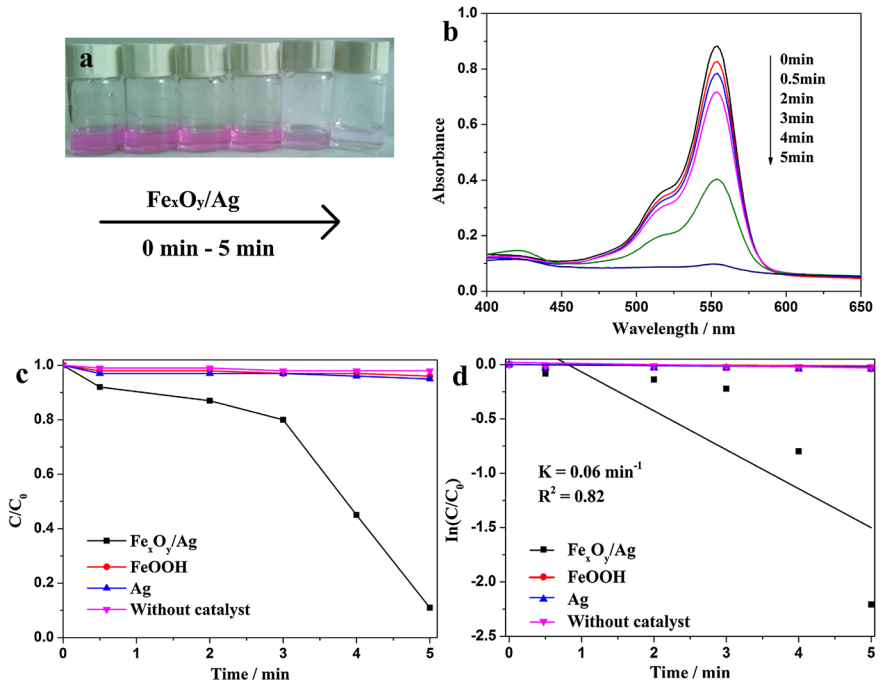

Fig. 7 **a** The photos of the corresponding solutions at various times. **b** UV–visible spectra for the chemical reduction of Rhodamine B using Fe_xO_y/Ag nanocomposites as catalyst. **c** Plot of C/C_0 versus reaction time for the reduction of Rhodamine B. **d** Relationship between $\ln(C/C_0)$ and reaction time t for the reduction using different catalysts

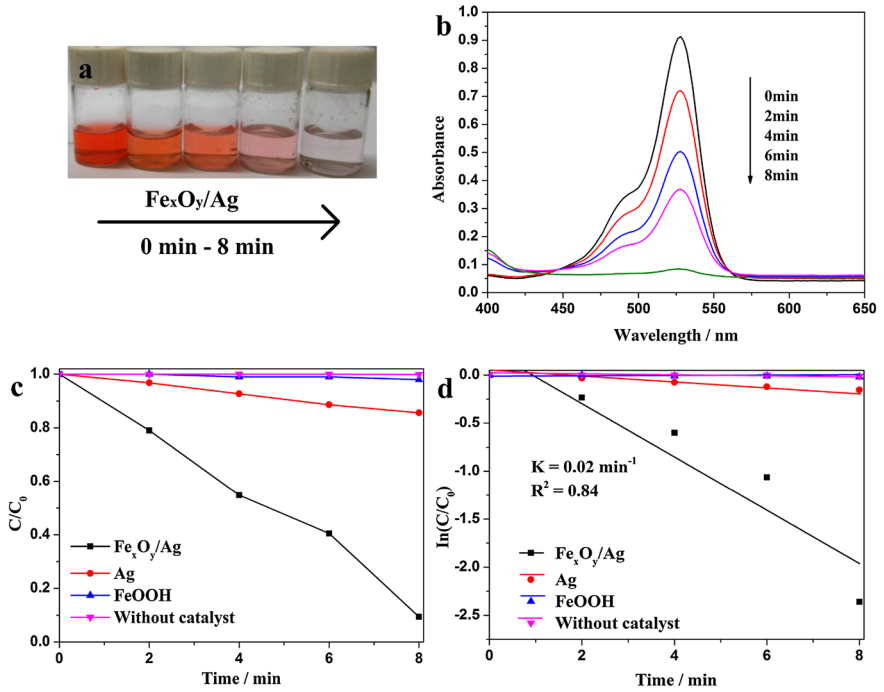

Fig. 8 **a** The photos of the corresponding solutions at various times. **b** UV–visible spectra for the chemical reduction of Rhodamine 6G using Fe_xO_y/Ag nanocomposites as catalyst. **c** Plot of C/C_0 versus reaction time for the reduction of Rhodamine 6G. **d** Relationship between $\ln(C/C_0)$ and reaction time t for the reduction using different catalysts

Conclusion

In this study, the Fe_xO_y /Ag nanocomposite was successfully prepared using a new and simple method. The citrate was polymerized on the FeOOH nanorod surface and the FeOOH nanorod was embedded within the citrate ions with negative charges situated outside, which is profitable for anchoring silver ions by electrostatic interaction. Subsequently, the silver ions were reduced by $NaBH_4$ in one step. Goethite nanorods provide an opportunity for heterogeneous catalysis through the incorporation with monodispersed Ag nanoparticles. The size and coverage of the Ag nanoparticles supported on the surface of Fe_xO_y can be easily controlled by varying the molar ratio of $AgNO_3$ and FeOOH. Our synthesized Fe_xO_y /Ag nanocomposites exhibited the high catalytic activity for the reduction of aromatic nitro compounds and organic dyes.

Acknowledgments The authors thank the National Natural Science Foundation of China (Grants 21001004, 20975001), and Prof. Yonghong Ni for data discuss.

References

1. Q. Zhang, S. Cai, L. Li, Y. Chen, H. Rong, Z. Niu, J. Liu, W. He, and Y. Li (2013). *ACS Catal.* **3**, 1681.
2. J. Han, Y. Liu, and R. Guo (2009). *J. Am. Chem. Soc.* **131**, 2060.
3. Ch V Rao and B. Viswanathan (2010). *J. Phys. Chem. C.* **114**, 8661.
4. L. Zhang, X. Y. Lang, A. Hirata, and M. W. Chen (2011). *ACS Nano.* **5**, 4407.
5. A. Lee, G. F. S. Andrade, A. Ahmed, M. L. Souza, N. Coombs, E. Tumarkin, K. Liu, R. Gordon, A. G. Brolo, and E. Kumacheva (2011). *J. Am. Chem. Soc.* **133**, 7563.
6. J. Jain, S. Arora, J. M. Rajwade, P. Omray, S. Khandelwal, and K. M. Paknikar (2009). *Mol. Pharm.* **6**, 1388.
7. P. Singh and D. A. Buttry (2012). *J. Phys. Chem. C.* **116**, 10656.
8. H. Wu, X. Huang, M. Gao, X. Liao, and B. Shi (2011). *Green Chem.* **13**, 651.
9. R. Narayanan and M. A. El-Sayed (2004). *J. Am. Chem. Soc.* **126**, 7194.
10. A. Roucoux, J. Schulz, and H. Patin (2002). *Chem. Rev.* **102**, 3757.
11. L. Ai, H. Yue, and J. Jiang (2012). *J. Mater. Chem.* **22**, 23447.
12. P. Zhang, C. Shao, and X. Li (2013). *Phys. Chem. Chem. Phys.* **15**, 10453.
13. N. Du, H. Zhang, and J. Yu (2009). *Chem. Mater.* **21**, 5264.
14. Z. Deng, H. Zhu, and B. Peng (2012). *ACS Appl. Mater. Interfaces* **4**, 5625.
15. A. Niu, Y. Han, and J. Wu (2010). *J. Phys. Chem. C.* **114**, 12728.
16. W. Jiang, Y. Zhou, and Y. Zhang (2012). *Dalton Trans.* **41**, 4594.
17. L. Ai, C. Zeng, and Q. Wang (2011). *Catal. Commun.* **14**, 68.
18. Z. Zhang, C. Shao, and Y. Sun (2012). *J. Mater. Chem.* **22**, 1387.
19. L. Mazeina and A. Navrotsky (2007). *Chem. Mater.* **19**, 825.
20. B. Tang, G. Wang, L. Zhuo, J. Ge, and L. Cui (2006). *Inorg. Chem.* **45**, 5196.
21. F. Meng, S. A. Morin, and S. Jin (2011). *J. Am. Chem. Soc.* **133**, 8408.
22. M. Lin, L. Tng, T. Lim, M. Choo, J. Zhang, H. R. Tan, and S. Bai (2014). *J. Phys. Chem. C.* **118**, 10903.
23. F. J. Berry, O. Helgason, A. Bohorquez, J. F. Marco, J. McManus, E. A. Moore, S. Mùrup, and P. G. Wynn (2000). *J. Mater. Chem.* **10**, 1643.
24. D. C. Rocchiccioli, R. Franck, V. Cabuil, and R. Massart (1987). *J. Chem. Res.* **5**, 126.
25. S. Kang and B. Xing (2008). *Langmuir* **24**, 2525.
26. C. R. Evanko and D. A. Dzombak (1998). *Environ. Sci. Technol.* **32**, 2846.
27. P. Makie, G. Westin, P. Persson, and L. Osterlund (2011). *J. Phys. Chem. A.* **115**, 8948.
28. M. Ali (1996). *Environ. Sci. Technol.* **30**, 1061.
29. K. Kandori, M. Fukuoka, and T. Ishikawa (1991). *J. Mater. Sci.* **26**, 3313.
30. H. Marcussen, P. E. Holm, B. W. Strobel, and H. C. B. Hansen (2009). *Environ. Sci. Technol.* **43**, 1122.
31. M. S. Calvar, J. Pacifico, J. P. Juste, and L. M. L. Marzán (2008). *Langmuir* **24**, 9675.
32. Y. Li, Y. Wu, Y. Gao, S. Sha, J. Hao, G. Cao, and C. Yang (2013). *RSC Adv.* **3**, 26361.
33. T. Y. Zhang, W. Q. Li, S. Z. Kang, L. X. Qin, G. D. Li, and J. Mu (2014). *J. Mater. Chem. A* **2**, 2952.
34. V. Reddy, R. S. Torati, S. Oh, and C. Kim (2013). *Ind. Eng. Chem. Res.* **52**, 556.
35. X. Wang (2004). Unpublished PhD Dissertation, Tsinghua University.
36. X. Song and J. F. Boily (2012). *Phys. Chem. Chem. Phys.* **14**, 2579.
37. G. M. Hernandez, P. Beck, F. Renard, E. Quirico, B. Lanson, R. Chiriac, and N. Findling (2011). *Cryst. Growth Des.* **11**, 2264.
38. C. Kind and C. Feldmann (2011). *Chem. Mater.* **23**, 4982.
39. P. Zhang, C. Shao, Z. Zhang, M. Zhang, J. Mu, Z. Guo, and Y. Liu (2011). *Nanoscale* **3**, 3357.
40. X. Du, J. He, J. Zhu, L. Sun, and S. An (2012). *Appl. Surf. Sci.* **258**, 2717.
41. G. Chang, Y. Luo, W. Lu, X. Qin, A. M. Asiri, A. O. A. Youbi, and X. Sun (2012). *Catal. Sci. Technol.* **2**, 800.
42. C. Wang, K. Tang, D. Wang, Z. Liu, and L. Wang (2012). *J. Mater. Chem.* **22**, 22929.